Supporting Information

Tunable, UV-shielding and biodegradable composites based on well-characterized lignins and Poly(butylene adipate-*co*-terephthalate)

Han-Min Wang,[a] Bin Wang,[a] Tong-Qi Yuan,[a] Lu Zheng,[b] Quentin Shi,[b] Wang Shuang-Fei,[c] Guo-Yong Song*[a] , Run-Cang Sun*[d]

[a]Beijing Key Laboratory of Lignocellulosic Chemistry, Beijing Forestry University, No. 35 Tsinghua East Road, Haidian District, Beijing 100083, China

[b]Shanghai Dssun New Material Co., Ltd. Shanghai 200223, China

[c]College of Light Industry and Food Engineering, Guangxi University, No. 100 Daxue East Road, Nanning 530004, China

[d]Liaoning Key Laboratory of Lignocellulose Chemistry and BioMaterials, Dalian Polytechnic University, No. 1 Qinggongyuan, Ganjingzi District, Dalian 116034, China

Email address:

Corresponding author: songg@bjfu.edu.cn, rcsun3@dlpu.edu.cn.

Contents

S1. Structural characteristics of HL during HTP process

The dramatic cleavage of β-*O*-4 linkages was considered as the favorable reaction during HTP, which was usually along with the formation of new condensed C-C bonds.[1,2] For example, the slightly increase of β-5 linkages occurred in the HL obtained from HTP in the present study. Meanwhile, the S/G ratio of HL (5.0) exhibited the elevated tendency as compared with that of DEL (2.9). For the purpose of quantifying the detailed functional groups of lignin during the HTP, the ^{31}P NMR spectra (Fig. S1) was performed and the amounts of OH and carboxylic groups were listed in Table S2. The contents of phenolic OH (S and G-types) and carboxylic groups were increased with the implementation of HTP process, whereas the number of aliphatic OH was decreased. For one thing, the enhancement of phenolic OH abundances in HL was mainly originated from the cleavage of β-*O*-4 linkages under the given condition. For another, the lower amounts of aliphatic OH were mostly derived from the oxidation reaction, which converted the aliphatic OH into carboxylic group at high temperatures. This oxidation reaction is more likely to occur at the side chains of lignin with lower molecular weights and further enriched the abundance of carboxylic group.[3] Therefore, in the present study, the lignin (HL) that was recovered from HTP showed the lower molecular weight and abundant hydroxyl groups as well as low polydispersity could provide the crucial opportunity for the conversion of the lignin into polymer material.

S2. Methods

Microwave-assisted lignin esterification reaction

In detail, HL and different acyl chloride reagents (calculated amounts) were firstly mixed in a round bottom flasks under continuous stirring, then the pyridine or TEA (or pyridine and TEA together) was added under ice water bath, finally the adequately mixed systems were heated to 80 ^{o}C (600 W) in the microwave synthesis labstation (Milestone MicroSYNTH, Italy) and kept for 0.5 h (The adopted temperature and reaction time were optimized from the preliminary experiment). As a control, these esterification reactions of lignin were also performed under no catalyst condition. Once the desired reaction time reached, ethanol was added into the resultant mixtures to terminate reaction and sufficient water was subsequently added to precipitate the esterified lignins. After the removal of solvent under vacuum, the esterified lignin preparations (ACL: acetyl chloride lignin, CCL: caprylyl chloride lignin, LCL: lauryl chloride lignin, and OCL: oleoyl chloride lignin) were washed with water and freeze-dried.

Characterization of UV−vis absorption and water contact angles of lignin preparations

In order to intuitively observe the effect of structural changes on ultraviolet absorption of lignin, the UV−vis absorption spectra of HL and esterified lignin preparations (ACL, CCL, LCL and OCL) were recorded by an ultraviolet spectrophotometer (TU1901, Beijing Purkinje General Instrument Co., Ltd.). The lignin samples were dissolved in 1,4-dioxane (0.04g/L in dioxane) and then all the lignin solutions were scanned at the same wavelength range of 250−700 nm to acquire the spectra. In addition, it is known that the hydrophobicity of lignin could be improved by proper modification, such as lignin esterification reaction. In an effort to insight into the hydrophobicity of HL before and after esterification reaction, the water contact angles of HL and esterified lignin preparations were recorded and analyzed on a KINO SL200KS Instrument by sessile drop technique on the surface of

dried lignin thin layer. Each sample was conducted at least three measurements and the average values were reported.

Molecular dynamics (MD) simulation

In this study, molecular dynamics (MD) simulation was typically performed to elucidate the dynamic compatibility of lignin (30 wt% loading of HL, LCL and OCL) and PBAT by using GROMACS 5.1.4 package. Firstly, the potential structures of HL, LCL and OCL have been constructed based on the characterized structural information (such as S/G ratios, molecular weight and abundances of linkages). In calculation modeling, the PBAT polymer contained 50-unit cells is initially established. The condensed-phased-optimized molecular potential for atomistic[4] simulation studies force field has been employed to optimize. In addition, the structure size of integrated polymers for PBAT/HL, PBAT/LCL and PBAT/OCL is 27.51Å ×27.51Å ×27.51Å. To obtain a global minimum energy configuration, a geometry optimization is first performed using the method of conjugate-gradient with convergence criteria (0.0001 kcal/mol).[5] The cells are then allowed to equilibrate over NPT simulations (isothermal-isobaric ensemble) at a room temperature of 300 K for 20 ns with a time step of 1 fs. The designed molecular systems of the polymer matrix can be obtained after a dynamics simulation under different temperatures (353 K, 373 K,403 K, 423 K and 473 K). These simulation processes are aimed to remove internal stresses in the cells using GROMACS 5.1.4 package. Next, a potential cutoff radius of 2.25 nm is applied in the calculation of the non-bonded interaction. Andersen feedback thermostat[6] and Berendsen barostat algorithm[7] are applied in the system temperature and pressure conversion. The Ewald summation method[8] with an accuracy of 0.001 kcal/mol is used in calculations of the interaction energy. Finally, the interaction energy (E) of the polymeric matrix is calculated by the following formulas:

$$E_N=E_{abN}-E_{aN}-E_{bN} \quad (1)$$

$$E_V=E_{abV}-E_{aV}-E_{bV} \quad (2)$$

$$E_P=E_{abP}-E_{aP}-E_{bP} \quad (3)$$

Where E_N, E_V and E_P represent Non-bond energy (KJ mol^{-1}), Van der Waals energy

(KJ mol^{-1}) and Electrostatic potential Energy (KJ mol^{-1}), respectively. E_{abN}, E_{abV} and E_{abP} represent Non-bond energy (KJ mol^{-1}), Van der Waals energy (KJ mol^{-1}) and Electrostatic potential Energy (KJ mol^{-1}) of PBAT/HL, PBAT/LCL or PBAT/OCL. E_{aN}, E_{aV} and E_{aP} represent Non-bond energy (KJ mol^{-1}), Van der Waals energy (KJ mol^{-1}) and Electrostatic potential Energy (KJ mol^{-1}) of PBAT. E_{aN}, E_{aV} and E_{aP} represent Non-bond energy (KJ mol^{-1}), Van der Waals energy (KJ mol^{-1}) and Electrostatic potential Energy (KJ mol^{-1}) of HL, LCL or OCL.

References

1 L.-P. Xiao, Z. Lin, W.-X. Peng, T.-Q. Yuan, F. Xu, N.-C. Li, Q.-S. Tao, H. Xiang and R.-C. Sun, *Sustainable Chem. Processes*, 2014, **2**, 9.

2 H. Wang, B. Wang, D. Sun, Q. Shi, L. Zheng, S. Wang, S. Liu, R. Xia and R. Sun, ChemSusChem, 2019, 12, 1059-1068.

3 C. Gioia, G. Lo Re, M. Lawoko and L. Berglund, J. Am. Chem. Soc., 2018, 140, 4054-4061.

4 Rigby, David , H. Sun , and B. E. Eichinger. *Polym. Int.*, 2015, 44,311-330.

5 Polyak B T . *Comput. Math. Math. Phys.*, 1969, 9, 94-112.

6 Andersen, Hans C ., *J. Chem. Phys.* 1980, 72, 2384-2393.

7 Berendsen, H. J. C. , Postma, J. P. M. , Van Gunsteren, W. F. , Dinola, A. , Haak, J. R. *J. Chem. Phys.,* 1998,81, 3684-3690.

8 Ewald, Paul Peter. *Ann. Phys.*, 1921, 369, 253.

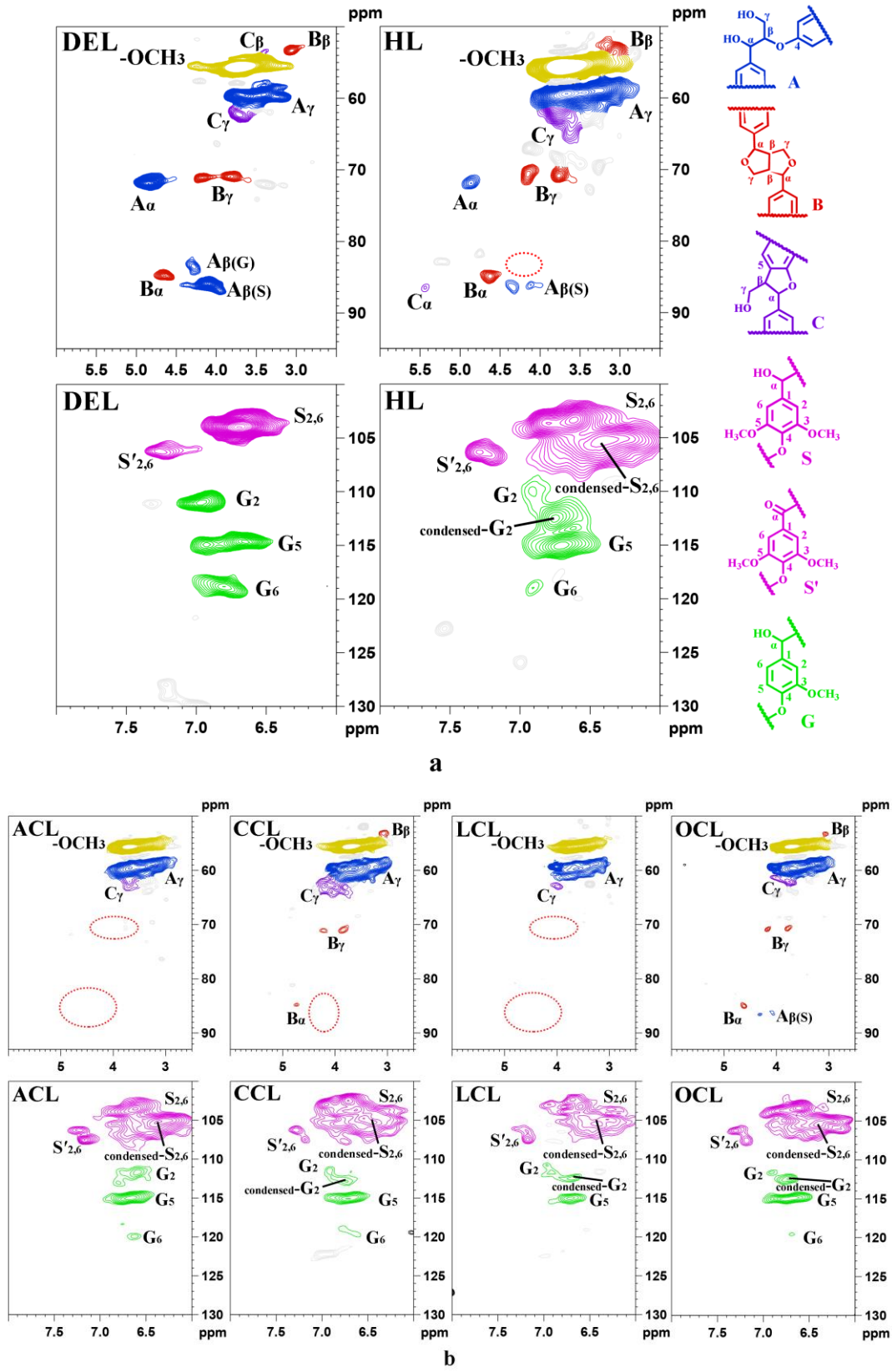

Fig. S1. Side-chain and aromatic regions in 2D-HSQC NMR spectra of lignin preparations (**a**) before and after HTP as well as (**b**) esterification reaction.

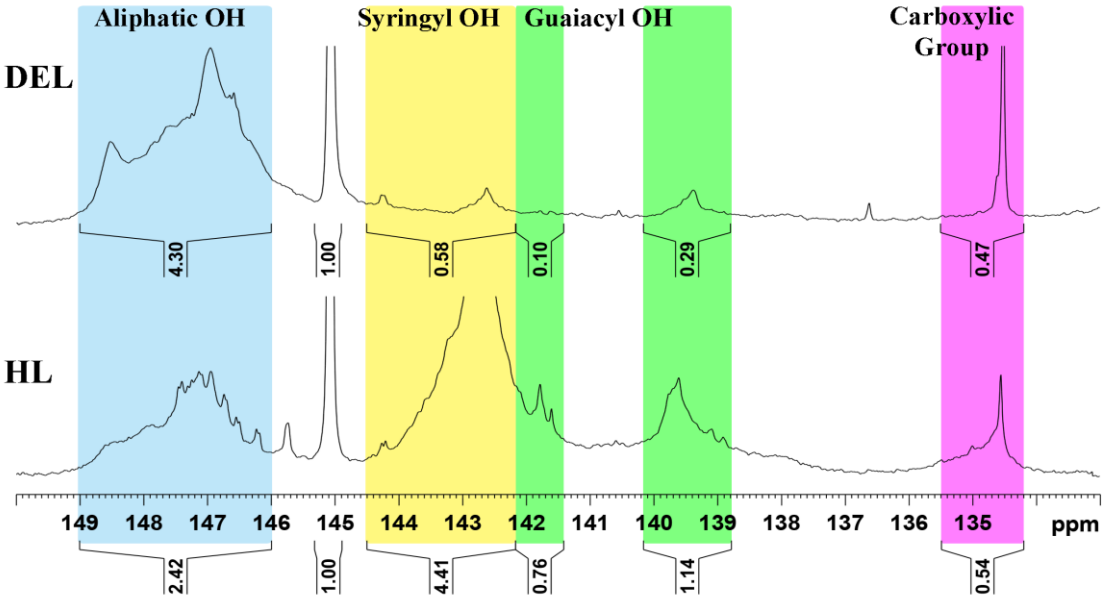

Fig. S2. Quantitative ^{31}P NMR spectra of DEL and HL as well as chemical shifts of the functional groups.

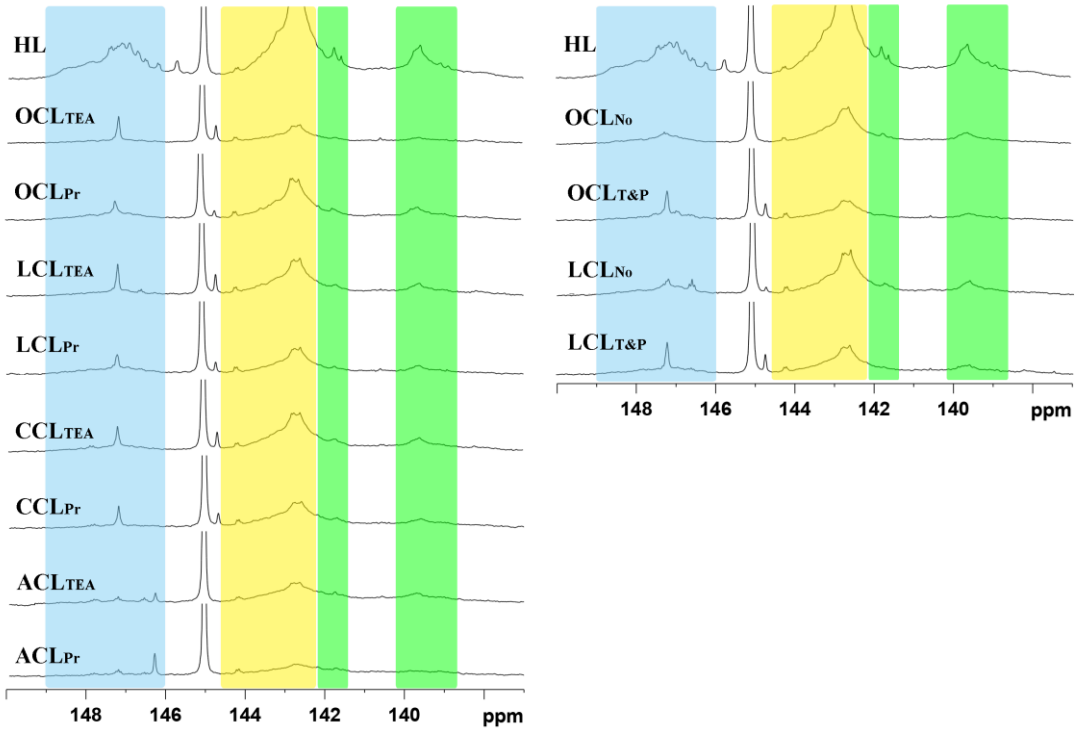

Fig. S3. ^{31}P NMR spectra of lignin preparations before and after esterification reaction.

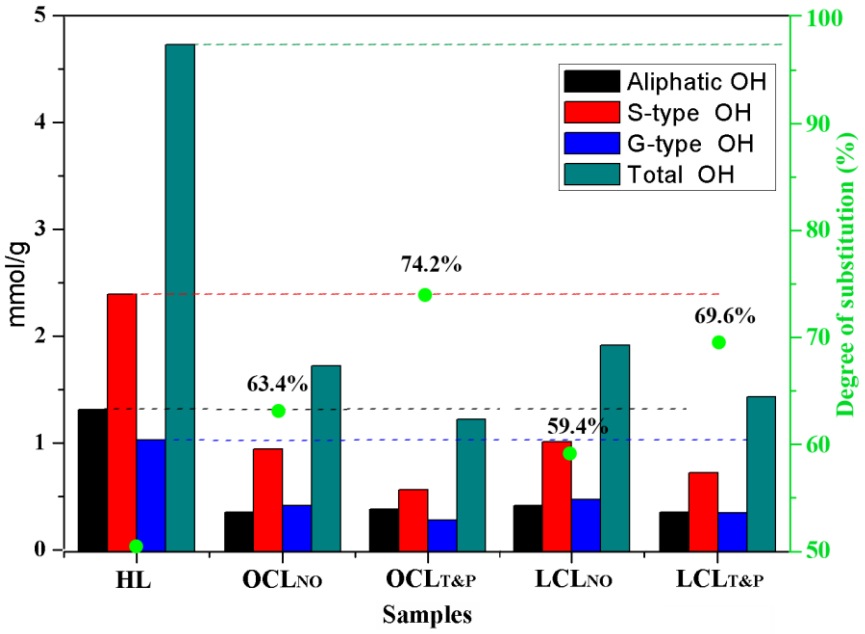

Fig. S4. The hydroxyl contents and degrees of substitution (DS, %) of lignin preparations before and after esterification reaction (with or without catalysts) based on quantitative ^{31}P NMR spectra.

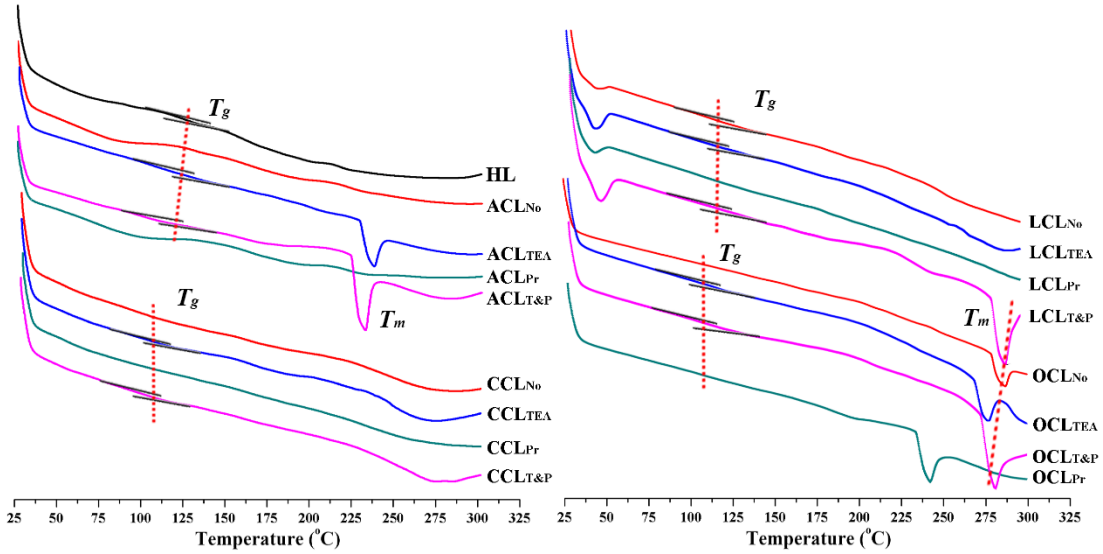

Fig. S5. DSC thermograms of lignin preparations before and after esterification reaction (T_g: glass transition temperature, T_m: melting temperature).

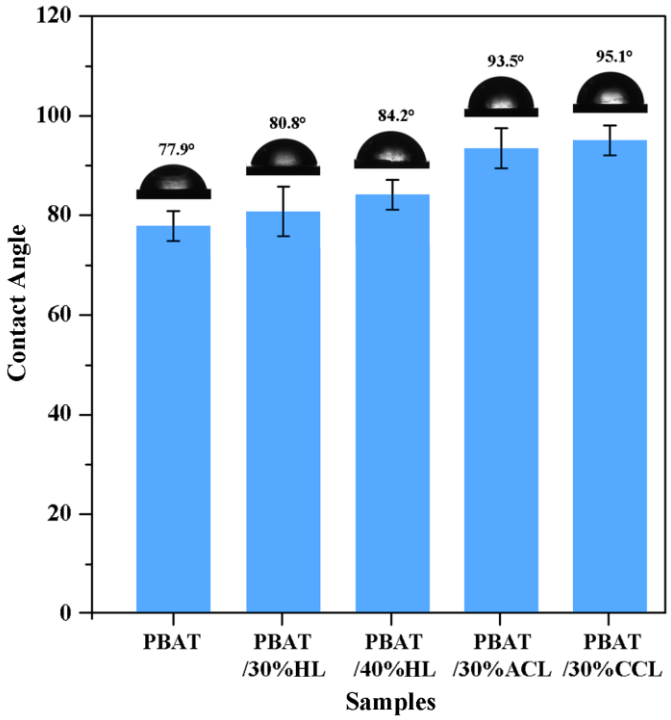

Fig. S6. Contact angles of neat PBAT and PBAT/lignin composite films

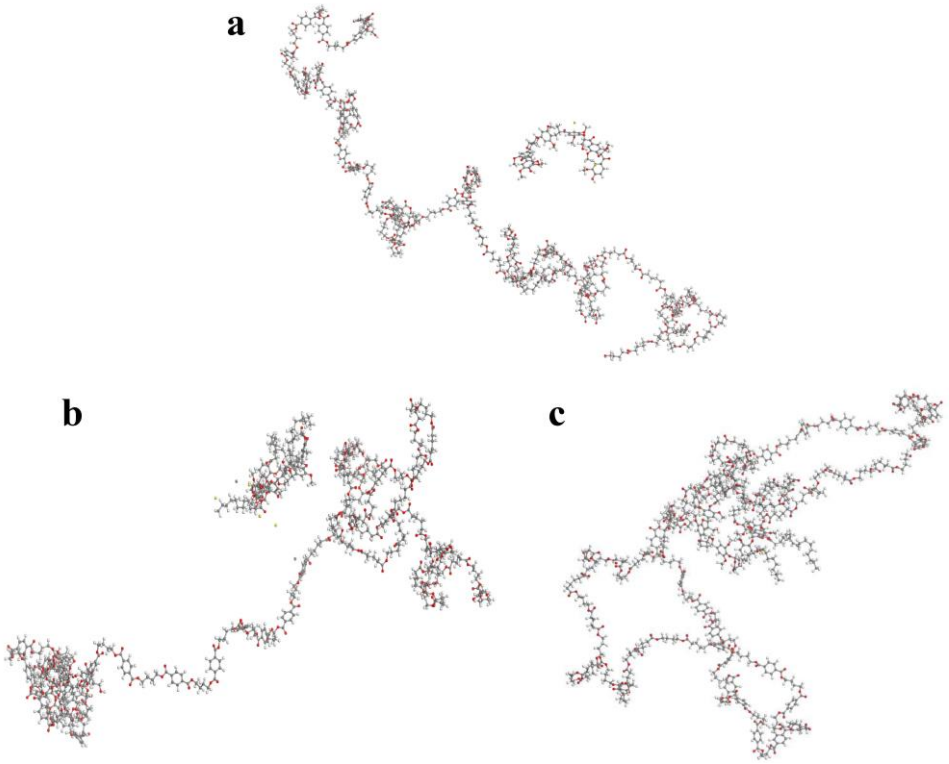

Fig. S7. Chemical structures of the simulated lignin/PBAT composites (a: HL/PBAT, b: LCL/PBAT, c: OCL/PBAT)

Table S1. Quantification of the lignin preparations by quantitative 2D-HSQC NMR method.

Samples	β-*O*-4	β-β	β-5	S/G[c]
DEL	56.67[a]	11.78	Tr[b]	2.9
HL	3.18	3.60	0.76	5.0

[a]Results expressed per 100 Ar based on quantitative 2D-HSQC spectra.

[b]Tr: Trace. [c]S/G ratio obtained by this equation: S/G ratio = $0.5I(S_{2,6})/I(G_2)$

Table S2. Quantification of the lignin preparations before and after HTP by quantitative ^{31}P-NMR spectra (mmol/g).

Samples	Aliphatic OH	Syringyl OH	Guaiacyl OH		Total OH	Carboxylic Group
			C[a]	NC[b]		
DEL	2.33	0.31	0.06	0.16	2.86	0.26
HL	1.31	2.39	0.41	0.62	4.73	0.29

[a]C: Condensed, 5-substitued lignin.

[b]NC: Not condensed.

Table S3. Thermogravimetric analysis (thermal decomposition temperature (T_d) and char residual at 600 °C) and glass transition temperature (T_g) of the lignin before and after esterification.

Samples	TGA		DSC
	T_d (℃)	Char (%)	T_g (℃)
HL	286.6	47.1	128.5
ACL	214.7	45.1	119.4
CCL	215.6	43.2	108.6
LCL	190.2	15.9	113.1
OCL	213.4	20.8	107.2

Table S4. Comparison of tensile properties of neat PBAT and PBAT/lignin composites without MAH.

Entry	Samples	ε elongation at break (%)	σ tensile strength (MPa)	E Young's modulus (MPa)	Rate of change (%)	
					ε	σ
1	PBAT	828.7±95.5	23.0±4.8	44.7±3.1	/	/
2	PBAT/30%HL	117.0±16.6	10.9±0.3	103.6±6.1	-85.9%[a]	-52.6%[a]
3	PBAT/40%HL	32.8±8.3	9.2±1.1	91.7±15.5	-96.0%[a]	-60.0%[a]
4	PBAT/30%ACL	108.0±1.3	11.5±0.2	82.0±9.2	-7.7%[b]	5.5%[b]
5	PBAT/30%CCL	290.3±22.5	11.5±0.3	60.2±3.4	148.1%[b]	5.5%[b]
6	PBAT/30%LCL	255.7±62.4	10.7±2.1	65.1±15.0	118.5%[b]	-1.8%[b]
7	PBAT/30%OCL	36.8±4.4	7.3±0.4	61.6±8.4	-68.5%[b]	-33.0%[b]

[a]: Compared with Entry 1, [b]: Compared with Entry 2.

※All the average values and standard deviation are calculated based on 4−6 duplication.

Table S5. DSC results of neat PBAT and PBAT/30 wt% lignin composites

Samples	DSC	
	T_g (°C)	T_m (°C)
PBAT	-35.2	135.5
PBAT/30%HL	-33.5	134.2
PBAT/30%ACL	-31.6	135.9
PBAT/30%CCL	-34.2	135.4
PBAT/30%LCL	-36.4	133.5
PBAT/30%OCL	-36.6	133.0

Table S6. The Non-bond Energy (KJ mol^{-1}) of the polymers and composites

Temperature (K)	353	373	403	423	473
OCL	-73.782	-98.564	-68.234	-56.085	-75.915
LCL	-99.124	-112.981	-134.752	-89.369	-79.403
HL	-81.254	-99.357	-113.703	-101.274	-83.782
PBAT	-2148.454	-2432.716	-2627.217	-2012.126	-1990.897
HL-PBAT	-1911.584	-2135.719	-2277.644	-1702.949	-1698.259
OCL-PBAT	-1677.891	-2109.107	-2051.067	-1580.039	-1665.537
LCL-PBAT	-1905.451	-2134.413	-2269.822	-1629.814	-1697.885

Table S7. The Van der Waals Energy (KJ mol^{-1}) of the polymers and composites

Temperature(K)	353	373	403	423	473
OCL	102.534	208.967	212.056	129.376	148.064
LCL	141.200	291.200	321.200	279.200	298.210
HL	97.123	117.172	165.421	191.347	143.531
PBAT	-2224.647	-2034.512	-1982.353	2358.561	1986.617
HL-PBAT	-1830.252	-1565.173	-1389.218	-1765.857	-1525.225
OCL-PBAT	-1822.401	-1455.764	-1318.17	-1807.433	-1451.186
LCL-PBAT	-1782.321	-1375.614	-1223.431	-1668.114	-1366.641

Table S8. The Electrostatic potential Energy (KJ mol^{-1}) of the polymers and composites

Temperature(K)	353	373	403	423	473
OCL	47.919	46.284	56.721	39.461	42.149
LCL	63.417	74.92	85.312	64.134	69.717
HL	31.417	39.112	52.783	55.715	41.152
PBAT	272.372	303.872	313.812	330.353	389.012
HL-PBAT	322.146	382.131	432.346	437.304	462.342
OCL-PBAT	351.538	397.339	453.994	440.939	486.873
LCL-PBAT	358.176	428.374	477.491	458.268	501.107